

# Phase transition of ultracold atoms immersed in a BEC vortex lattice

R. H. Chaviguri,<sup>1</sup> T. Comparin,<sup>2</sup> V. S. Bagnato,<sup>1</sup> and M. A. Caracanhas<sup>1</sup>

<sup>1</sup>*Instituto de Física de São Carlos, Universidade de São Paulo, C.P. 369, São Carlos, SP, 13560-970, Brazil*

<sup>2</sup>*Laboratoire de Physique Statistique, École Normale Supérieure/PSL Research University, UPMC, Université Paris Diderot, CNRS, 24 rue Lhomond, 75005 Paris, France*

(Dated: March 11, 2022)

We investigate the quantum phases of ultracold atoms trapped in a vortex lattice using a mixture of two bosonic species (A and B), in the presence of an artificial gauge field. Heavy atoms of species B are confined in the array of vortices generated in species A, and they are described through a Bose-Hubbard model. In contrast to the optical-lattice setups, the vortex lattice has an intrinsic dynamics, given by its Tkachenko modes. Including these quantum fluctuations in the effective model for B atoms yields an extended Bose-Hubbard model, with an additional “phonon”-mediated long-range attraction. The ground-state phase diagram of this model is computed through a variational ansatz and the quantum Monte Carlo technique. When compared with the ordinary Bose-Hubbard case, the long-range interatomic attraction causes a shift and resizing of the Mott-insulator regions. Finally, we discuss the experimental feasibility of the proposed scheme, which relies on the proper choice of the atomic species and on a large control of physical parameters, like the scattering lengths and the vorticity.

PACS numbers: 03.75.Kk, 67.85.De, 71.38.-k

## I. INTRODUCTION

Two-component condensate systems had an enormous impact in the field of ultracold atoms, especially since the experimental realization of a Bose-Einstein condensate (BEC) of fermions. This consists of effective bosonic molecules, the tightly bound Cooper pairs, formed after the fermions be sympathetically cooled by another bosonic or fermionic atomic species. The experimental observation of the BEC-BCS crossover with this molecular BEC [1] proved once more the relevance of ultracold atoms as a powerful tool to test condensed-matter models, which can be studied in a highly controllable environment [2, 3]. The two-species BEC of bosonic atoms also has rich physics to be explored. An important experiment performed in Cornell’s group, with different <sup>87</sup>Rb hyperfine states, addressed the static properties of binary mixtures, their relative phase coherence and their dynamics [4]. The same group was able to nucleate vortices in this system [5], and, more recently, to produce the superposition of vortex-lattice BECs [6].

The vortex configuration in BEC was predicted by Feynman [7], who suggested that a superfluid can rotate when pierced by an array of quantized singularities or vortices. In 1969, Tkachenko proposed that a vortex lattice in a superfluid would support transverse elastic-modes [8]. He showed that a triangular lattice has the lowest energy of all simple lattices with one vortex per unit cell, and that it is stable for all normal modes. These predictions were experimentally realized with dilute BEC gases in 2001 [9], and followed by the observation of vortex-line oscillations, that is, the low-energy Tkachenko modes [10]. Once established, the vortex-lattice configuration proved to be stable, including its normal modes, for a range of rotation frequencies close to, but below that of the external trap confining potential [11, 12].

In a previous work [13], we considered a neutral impurity immersed in a vortex lattice, interacting with the Tkachenko modes. We addressed the shallow-lattice regime, assuming a quadratic energy dispersion for the impurity species, and taking the continuous limit for its momentum. In this work, an analogous system is studied in the tight-binding regime, where heavy atoms (impurities) are strongly trapped in the sites of the vortex lattice formed by condensed bosons of another species. This vortex-lattice setup should be compared to the technique of trapping ultracold atoms in optical lattices generated by laser beams. The study of bosonic atoms in optical lattices led to the breakthrough observation of the quantum phase transition between the superfluid and Mott-insulating phases [14], well described by the Bose-Hubbard (BH) model for lattice bosons [15].

Important results obtained with optical lattices rely on the fact that these are rigid (i.e., do not support phonons [16]) and free of defects. To better simulate the condensed-matter models for solid-state crystals, however, a recent trend has been to introduce artificial dynamics in these light crystals [17–19]. In our proposed scheme, the dynamics emerges naturally through the normal-modes excitations of the vortex lattice. The effective Hamiltonian for the lattice-confined impurities corresponds to a polaronic Bose-Hubbard (BH) model, with parameters that are modified by the lattice dynamics, notably by the introduction of a long-range “phonon”-mediated interaction.

The generalization of BH models in the ultracold atoms context is connected to the use of atoms with strong dipole moment, for which the strength of interatomic interaction decays slowly with the distance [20]. In this case, the system is described through an extended Bose-Hubbard (EBH) model, with the additional long-range interaction generating a rich variety of phases. For the

one-dimensional case, the phase diagram includes the peculiar Haldane-insulator phase [21]. In two dimensions, the predicted phases range from density-wave to supersolidity [22, 23]. Ref. [24], in particular, reports the experimental realization of a EBH model in three dimensions.

The vortex-lattice setup proposed here also realizes a EBH models, due to the effective long-range attraction generated by the lattice dynamics. Similarly to optical lattices, the high and independent control of the system parameters would allow one to explore the quantum phases of impurities in a vortex lattice. The relevant experimental methods include the use of Feshbach resonances to tune atomic scattering lengths [25] and of the selective absorption-image technique to characterize the quantum-state configuration [3, 26, 27].

This paper is structured as follows: Sec. II presents the derivation of an effective Bose-Hubbard model for impurity atoms trapped by the vortex lattice of the other atomic species. The phase diagram of this model is determined through the quantum Monte Carlo technique, and compared to the existing results (*cf.* Sec. III). In Sec. IV, we give a beyond mean-field treatment for species A, which leads to the EBH model for impurity atoms, including long-range interactions. The phase diagram of this “dynamical” model is analyzed in Sec. V. In Sec. VI, we describe the physical parameters relevant for an experimental realization of our proposal, and the main conclusions are reported in VII.

## II. PHYSICAL MODEL

We consider a two-component mixture of species A and B, in a quasi-2D geometry. The vortex lattice in species A is excited by the artificial-gauge-field technique [28], where the internal atomic structure is carefully engineered by the optical potentials to produce Berry phases and nucleate vortices [29]. The main idea is to replace the rotating trap mechanism by using an artificial vector potential  $\mathbf{A}$ , which selectively couples to A atoms and does not affect species B. The Hamiltonian  $H$  of the system is the sum of the following three terms:

$$\begin{aligned} H_A &= \int d^2r \left[ \hat{\psi}_A^\dagger(\mathbf{r}) \frac{(-i\hbar\nabla - \mathbf{A}(\mathbf{r}))^2}{2m_A} \hat{\psi}_A(\mathbf{r}) + \right. \\ &\quad \left. + \hat{\psi}_A^\dagger(\mathbf{r}) V_{\text{ext}}(\mathbf{r}) \hat{\psi}_A(\mathbf{r}) + \frac{g_A}{2} \left( \hat{\psi}_A^\dagger(\mathbf{r}) \hat{\psi}_A(\mathbf{r}) \right)^2 \right], \\ H_B &= \int d^2r \left[ \hat{\psi}_B^\dagger(\mathbf{r}) \frac{(-i\hbar\nabla)^2}{2m_B} \hat{\psi}_B(\mathbf{r}) + \right. \\ &\quad \left. + \hat{\psi}_B^\dagger(\mathbf{r}) V_{\text{ext}}(\mathbf{r}) \hat{\psi}_B(\mathbf{r}) + \frac{g_B}{2} \left( \hat{\psi}_B^\dagger(\mathbf{r}) \hat{\psi}_B(\mathbf{r}) \right)^2 \right], \\ H_{AB} &= g_{AB} \int d^2r \hat{\psi}_A^\dagger(\mathbf{r}) \hat{\psi}_B^\dagger(\mathbf{r}) \hat{\psi}_A(\mathbf{r}) \hat{\psi}_B(\mathbf{r}), \end{aligned} \quad (1)$$

where species  $i \in \{A, B\}$  is described by the creation (destruction) field-operator  $\hat{\psi}_i^\dagger(\mathbf{r})$  ( $\hat{\psi}_i(\mathbf{r})$ ) at the two-dimensional position  $\mathbf{r} = (x, y)$ . The strength

of intra and inter-species repulsive contact interactions are given by  $g_i = 2\sqrt{2\pi}\hbar^2 a_i/m_i\ell_z^i$  and  $g_{AB} = \sqrt{2\pi}\hbar^2 a_{AB}/m_{AB}\ell_z^{AB}$ , respectively, where  $m_{AB} = m_A m_B / (m_A + m_B)$  is the reduced mass, and  $a_i$  and  $a_{AB}$  are the intra and inter-species s-wave scattering lengths. The length scales  $\ell_z^i = \sqrt{\hbar/(m_i\omega_z)}$  and  $\ell_z^{AB} = \sqrt{\hbar/(m_{AB}\omega_z)}$  are functions of the harmonic confining frequency  $\omega_z$  in the transverse direction. The vector potential  $\mathbf{A}$  determines the vorticity  $\Omega$  for the BEC A along the  $z$  axis through  $\Omega = |\nabla \times \mathbf{A}|/m_A$ . At a critical vorticity, the residual confining potential for A tends to zero [30]. For species B, the effect of the slowly-varying external trap potential  $V_{\text{ext}}(\mathbf{r})$  may be included through the Local Density Approximation.

Within a mean-field treatment of  $H_A$ , the vortex-lattice wave function for species A is built as the linear combination of degenerate lowest-Landau-levels solutions of the rotational Gross-Pitaevskii equation. This yields an Abrikosov lattice of vortices, encoded in the wave function  $\psi_A(\mathbf{r}) = \sqrt{n_A}\varphi_A(\mathbf{r})$ , where  $n_A = N_A/S$  is the average atomic density (with  $S$  being the surface area). The  $\mathbf{r}$ -dependent factor reads [30, 31]

$$\varphi_A(\mathbf{r}) = (2v)^{1/4} \vartheta_1(\zeta\sqrt{\pi v}, \rho) \exp \frac{\zeta^2 - |\zeta|^2}{2}, \quad (2)$$

where  $\zeta$  represents the complex variable  $(x + iy)/l_z^A$ ,  $\rho = \exp(i\pi\tau)$ ,  $\tau = u + iv$ ,  $u = -1/2$  and  $v = \sqrt{3}/2$ . The triangular lattice of vortices is formed by the zeros of the Jacobi theta function  $\vartheta_1$ .

For the stability of this vortex lattice we assume a vanishing temperature,  $T = 0$ . Then, in spite of not having a phase-coherent system, as part of the atoms A are outside the condensate state, we still have well established vortex-lattice density profile [32]. Moreover, we consider the mean-field quantum-Hall regime [31], with the number of vortices  $N_V$  well below the number of atoms in A, that is, a high ratio  $\nu = N_A/N_V \gg 1$ . In this regime, neither quantum nor thermal fluctuations affect the vortex-lattice stability. We also assume  $N_B \sim N_V \ll N_A$ , that allow us to disregard the effects of the dilute species on the stability of the vortex lattice.

In the above scenario, we can apply the Bogoliubov transformation in the field operator  $\hat{\psi}_A$  to derive the excitations around the vortex-lattice fundamental state, that is, to include the quantum fluctuations beyond the mean-field approximation for A:  $\hat{\psi}_A = \psi_A + \delta\hat{\psi}_A$ . We consider the grand-canonical formalism, with chemical potentials  $\mu_i$  for the species A and B, and rewrite the total system Hamiltonian in Eq. (1) as an expansion in powers of  $\delta\hat{\psi}_A$ . To the second-order, this expansion reads

$$K = \underbrace{H_B + H_{AB}^{(0)} - \mu_B \hat{N}_B}_{K_B} + \underbrace{H_{AB}^{(1)}}_{H_{\text{int}}} + \underbrace{H_A^{(2)} - \mu_A \hat{N}_A}_{K_A^{\text{BOG}}} \quad (3)$$

where  $\hat{N}_A$  and  $\hat{N}_B$  are the number operators for species A and B, and where the superscripts in  $H_A^{(2)}$ ,  $H_{AB}^{(0)}$  and

$H_{AB}^{(1)}$  indicate the order of the expansion. Considering the validity of the mean-field vortex-lattice solution for species A, the coefficient of the first order term  $H_A^{(1)}$  is zero. We truncate the interaction term  $H_{AB}$  to first order, and we do not show here the mean-field contribution to the energy of species A.

In this section we only consider the 0th order term in Eq. (3),  $K_B$ , in which species A appears as an effective mean-field potential for species B. The inter-species interaction term reads  $H_{AB}^{(0)} = \int d^2r V_A(\mathbf{r}) \hat{\psi}_B^\dagger(\mathbf{r}) \hat{\psi}_B(\mathbf{r})$ , where  $V_A(\mathbf{r}) = n_{AGAB} |\varphi_A(\mathbf{r})|^2$  with  $\varphi_A(\mathbf{r})$  given by Eq. (2), constitutes the static lattice potential seen by B atoms. In the dilute regime for species B (i.e., for  $N_B \ll N_A$ ), the repulsive interspecies interaction causes the localization of B atoms at the vortex-core positions, which is energetically favorable as the density of A atoms vanish there. This effect is at the basis of the derivation of an effective Bose-Hubbard model for B atoms, as detailed below.

We focus on the tight-binding regime, where the lattice depth  $V_0 = n_{AGAB}$  is much larger than the recoil energy  $E_r = \hbar^2/(2m_B \xi^2)$ .  $E_r$  is the natural energy-scale for B atoms trapped in a vortex core, with radius approximately equal to the healing length  $\xi (= \hbar/\sqrt{2m_A n_{AGA}})$  of the species A BEC. The parameter  $\Gamma_{LLL} = n_{AGA}/2\hbar\Omega$  is associated to the lowest-Landau-level constraint ( $\Gamma_{LLL} < 1$ , cf. Ref. [11]), and it connects with the vortex-lattice density  $n_V$  through  $n_V \sim 1/\pi d^2$ , where  $d = 2\sqrt{\hbar/(m_A \Omega)}$  is the inter-vortex separation [7, 12]. We assume that the energy-level spacing between the Bloch bands is large compared to the relevant energies of processes involving B atoms, which are then restricted to the lowest-energy band. The single-band assumption is especially valid in the tight-binding regime ( $V_0/E_r \gg 1$ ) considered in this work. This allows us to expand the field operator for species B in terms of Bloch wave functions:

$$\hat{\psi}_B(\mathbf{r}) = \sum_{\mathbf{k}} \Phi_{\mathbf{k}}(\mathbf{r}) \hat{b}_{\mathbf{k}}, \quad (4)$$

where  $\hat{b}_{\mathbf{k}}$  destroys a particle in a quasi-momentum state  $\mathbf{k}$ . The Wannier function  $\varphi_B(r_j)$ , defined through  $\Phi_{\mathbf{k}}(\mathbf{r}) = (1/\sqrt{N_V}) \sum_j \varphi_B(r_j) e^{i\mathbf{k} \cdot \mathbf{R}_j}$ , is localized at the vortex sites  $\mathbf{R}_j$  ( $r_j = |\mathbf{r} - \mathbf{R}_j|$ ) and is normalized to one. Expanding the field operator as a sum of Wannier functions in each lattice site, and considering only nearest-neighbor hopping and on-site interaction,  $K_B$  can be rewritten as a BH Hamiltonian [15]:

$$K_B = -J \sum_{\langle i,j \rangle} \hat{b}_i^\dagger \hat{b}_j + \frac{U}{2} \sum_i \hat{n}_i (\hat{n}_i - 1) - \mu_B \sum_i \hat{n}_i, \quad (5)$$

where  $\hat{b}_i = (1/\sqrt{N_V}) \sum_{\mathbf{k}} e^{i\mathbf{k} \cdot \mathbf{R}_i} \hat{b}_{\mathbf{k}}$ ,  $\hat{n}_i = \hat{b}_i^\dagger \hat{b}_i$ , and  $\langle i,j \rangle$  denotes nearest-neighbor pairs. The hopping coefficient and on-site repulsion strength are given respectively by

$$J = - \int d^2r \varphi_B^*(r_i) \left[ -\frac{\hbar^2 \nabla^2}{2m_B} + g_{AB} n_A |\varphi_A(\mathbf{r})|^2 \right] \varphi_B(r_j), \quad (6)$$

and

$$U = g_B \int d^2r |\varphi_B(r)|^4. \quad (7)$$

$U$  can be determined by assuming a Gaussian function for  $\varphi_B(r)$  ( $= |B_0| e^{-r^2/2\ell_0^2}$ ) [33], with  $\int d^2r |\varphi_B(r)|^2 = 1$  and width  $\ell_0^2 = \hbar \xi / \sqrt{m_B V_0}$  (harmonic approach for the vortex-core density profile [34]). This gives  $U = g_B / 2\pi \ell_0^2$ . On the other hand, the Gaussian ansatz leads to a poor approximation for  $J$ , which is better determined through the solution of a 1D Mathieu equation [35]. In analogy with the case of optical lattices, the resulting expression for  $J$  reads

$$J = \frac{4}{\sqrt{\pi}} E_r \left( \frac{V_0}{E_r} \right)^{\frac{3}{4}} \exp \left( -2 \sqrt{\frac{V_0}{E_r}} \right). \quad (8)$$

Using the vortex-lattice potential depth and recoil energy in the expressions for  $J$  and  $U$ , we obtain

$$\frac{U}{J} = \frac{1}{\sqrt{2}} \frac{a_B}{\ell_z^B} \left( \frac{a_A}{2a_{AB}} \frac{m_{AB}}{m_B} \right)^{1/4} e^{\sqrt{\frac{2a_{AB}}{a_A} \frac{m_B}{m_{AB}}}}. \quad (9)$$

In contrast with optical-lattice setups, where  $U/J$  is controlled by the laser-beam properties and atomic scattering length, in the vortex lattice this ratio is connected to the atomic properties through the inter- and intra-species scattering lengths ( $a_A$ ,  $a_B$ , and  $a_{AB}$ ), which can be independently controlled with uniform magnetic fields via the Feshbach-resonance technique [25]. The mapping in Eq. (9) opens the possibility of using the vortex-lattice setup described in this paper to explore the BH phase diagram on a triangular lattice, as will be shown in Sec. III.

### III. BOSE-HUBBARD PHASE DIAGRAM

At zero temperature, the Bose-Hubbard model in Eq. (5) features a phase transition between a Mott insulator (MI), with an integer number of atoms per site, and a phase-coherent superfluid (SF) phase [36]. The phase diagram has been characterized in detail, for several geometries and dimensionalities (see Ref. [37] for a review). For the two-dimensional triangular lattice, one can compute the phase boundaries at several levels of approximation. The simplest case consists in a mean-field approach [15]. By decoupling the kinetic part of Eq. (5) through  $\hat{b}_i^\dagger \hat{b}_j \simeq \langle \hat{b}_i^\dagger \rangle \hat{b}_j + \hat{b}_i^\dagger \langle \hat{b}_j \rangle - \langle \hat{b}_i^\dagger \rangle \langle \hat{b}_j \rangle$ , the Hamiltonian becomes a sum of single-site terms:  $K_B = \sum_i K_B^{(i)}$ . Assuming a real and homogeneous local order parameter  $\Psi = \langle \hat{b}_i \rangle$ , each term reads

$$K_B^{(i)} = -zJ\Psi(\hat{b}_i^\dagger + \hat{b}_i) + zJ\Psi^2 + \frac{U}{2} \hat{n}_i (\hat{n}_i - 1) - \mu_B \hat{n}_i, \quad (10)$$

where  $z$  is the number of neighbors per site ( $z = 6$ , for a triangular lattice). The first term in Eq. (10) is then treated through second-order perturbation theory

[36, 38]. We expand the resulting energy spectrum in powers of the order parameter  $\Psi$ , and apply Landau criterion to identify the phase transition [38]. The boundary between the superfluid phase and the Mott insulator with filling factor  $g$  is given by

$$\mu_B = \frac{U(2g-1) - zJ}{2} \pm \frac{\sqrt{U^2 - 2zUJ(2g+1) + z^2J^2}}{2}, \quad (11)$$

where the  $+$  ( $-$ ) sign refers to the upper (lower) boundary of the Mott-insulator lobe (*cf.* Fig. 1).

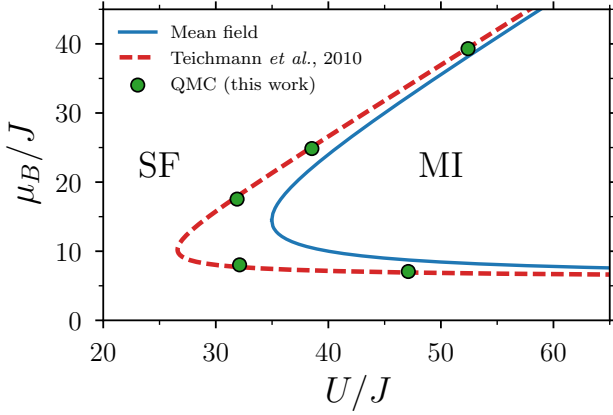


Figure 1. Phase boundary between the Mott-insulator lobe with filling factor  $g = 1$  (MI) and the superfluid phase (SF), on a two-dimensional triangular lattice. Different boundaries are obtained through mean-field theory (blue solid line, see Eq. (11)), process-chain approach (dashed red line, from Ref. [39]), and the quantum Monte Carlo technique (green circles, *cf.* Appendix B).

The mean-field phase diagram is known to underestimate the area of the Mott-insulator lobes. More accurate boundaries are obtained through the diagrammatic process-chain approach, where a perturbation series in  $J$  is computed up to high order. On the square lattice, this technique yields a phase diagram in extremely good agreement with unbiased quantum Monte Carlo (QMC) results [40]. Results of the process-chain approach are also available on the triangular lattice [39], for which the tip of the Mott-insulator lobe with filling  $g = 1$  is at  $(U/J, \mu_B/J)_{\text{crit}} \simeq (26.6, 10.2)$  – *cf.* Fig. 1.

We also study the triangular-lattice BH model through the worm-algorithm QMC technique [41, 42]. We extract the critical points through the finite-size-scaling analysis of the superfluid density (*cf.* Appendix B), and the numerical results are in good agreement with the process-chain phase boundary (see Fig. 1). In Sec. V, the same QMC algorithm is used to characterize the extended Bose-Hubbard model.

#### IV. VORTEX-LATTICE DYNAMICS

The model derived and characterized in Sections II and III does not include a peculiar aspect of the vortex-lattice physics, namely the intrinsic dynamics determined by its normal modes. The inclusion of these modes modifies the hopping amplitude and the interactions for B atoms. In addition to the trapping mechanism which keeps B atoms in the vortex lattice of A, we also consider the scattering of the B atoms by the Tkachenko modes of species A. In the following, we derive the effective BH Hamiltonian that follows from the inclusion of the lattice “vibrations”, i.e., the quantum fluctuations beyond the mean-field vortex-lattice solution in Eq. (2).

According to Eq. (3), the first-order term in powers of  $\delta\hat{\psi}_A$  yields [13]

$$H_{\text{int}} = g_{AB} \int d^2r \left[ \delta\hat{\psi}_A^\dagger \hat{\psi}_B^\dagger \hat{\psi}_B \psi_A + \psi_A^* \hat{\psi}_B^\dagger \hat{\psi}_B \delta\hat{\psi}_A \right]. \quad (12)$$

The second-order term, i.e., the Hamiltonian  $K_A^{\text{BOG}}$  for species A, is diagonalized through the Bogoliubov-mode expansion

$$\delta\hat{\psi}_A(\mathbf{r}) = \frac{1}{\sqrt{S}} \sum_{\mathbf{q}} [u_{\mathbf{q}}(\mathbf{r}) \hat{a}_{\mathbf{q}} - v_{\mathbf{q}}(\mathbf{r}) \hat{a}_{\mathbf{q}}^\dagger]. \quad (13)$$

This expansion leads to  $K_A^{\text{BOG}} = \sum_{\mathbf{q}} \epsilon_{\mathbf{q}} \hat{a}_{\mathbf{q}}^\dagger \hat{a}_{\mathbf{q}}$ , plus a constant term that only shifts the mean-field chemical potential. This expression is obtained for specific values of  $u_{\mathbf{q}}$  and  $v_{\mathbf{q}}$ , and it includes the operator  $\hat{a}_{\mathbf{q}}^\dagger$  ( $\hat{a}_{\mathbf{q}}$ ) which creates (annihilates) a Tkachenko-mode excitation with wave number  $\mathbf{q}$  and energy dispersion  $\epsilon_{\mathbf{q}}$  [31]. In analogy with the derivation of Eq. (5), we expand  $\hat{\psi}_B$  in Eq. (12) in terms of localized Wannier functions, which yields

$$K_B + H_{\text{int}} = -J \sum_{\langle i,j \rangle} \hat{b}_i^\dagger \hat{b}_j + \frac{U}{2} \sum_i \hat{n}_i (\hat{n}_i - 1) - \mu_B \sum_i \hat{n}_i + g_{AB} \sqrt{\frac{n_A}{S}} \sum_{\mathbf{q}, i, j} [\Lambda_{\mathbf{q}}^{ij} \hat{a}_{\mathbf{q}} + \bar{\Lambda}_{\mathbf{q}}^{ij} \hat{a}_{\mathbf{q}}^\dagger] \hat{b}_i^\dagger \hat{b}_j, \quad (14)$$

where

$$\Lambda_{\mathbf{q}}^{ij} = \int d^2r [\varphi_A^*(\mathbf{r}) u_{\mathbf{q}}(\mathbf{r}) - \varphi_A(\mathbf{r}) v_{\mathbf{q}}^*(\mathbf{r})] \varphi_B^*(r_i) \varphi_B(r_j),$$

$$\bar{\Lambda}_{\mathbf{q}}^{ij} = \int d^2r [\varphi_A(\mathbf{r}) u_{\mathbf{q}}^*(\mathbf{r}) - \varphi_A^*(\mathbf{r}) v_{\mathbf{q}}(\mathbf{r})] \varphi_B^*(r_i) \varphi_B(r_j). \quad (15)$$

$\Lambda_{\mathbf{q}}^{ij}$  is suppressed for large separations between sites  $i$  and  $j$ , and it can be approximately set to zero for  $|\mathbf{R}_i - \mathbf{R}_j|$  larger than  $d$  (nearest-neighbor approach) – *cf.* Appendix A. Here, however, we only consider the case of  $i = j$ , that is, we also neglect the nearest-neighbor pairs  $(i, j)$  in the sum in the last term of Eq. (14) (thus neglecting induced-tunneling terms).

The next step is to apply a unitary transformation in the total Hamiltonian given by Eq. (3), to cancel the

interaction term between impurities and lattice modes. This will be incorporated in the coefficients of the impurity BH Hamiltonian, providing an effective polaronic model [43, 44]. We consider

$$\tilde{H} = e^{-\mathcal{U}} H e^{\mathcal{U}} = H + [\mathcal{U}, H] + \frac{1}{2!} [\mathcal{U}, [\mathcal{U}, H]] + \dots, \quad (16)$$

with

$$\mathcal{U} = \frac{1}{\sqrt{S}} \sum_{\mathbf{q}, j} \frac{1}{\epsilon_q} [\alpha_{\mathbf{q}, j}^* \hat{a}_{\mathbf{q}}^\dagger - \alpha_{\mathbf{q}, j} \hat{a}_{\mathbf{q}}] \hat{n}_j. \quad (17)$$

The transformed Hamiltonian depends on how the impurity and lattice-modes operators are modified. For the real-space impurity operator, we have

$$e^{-\mathcal{U}} \hat{b}_i e^{\mathcal{U}} = \hat{b}_i \hat{X}_i, \quad (18)$$

with  $\hat{X}_i = e^{\hat{Y}_i}$  and  $\hat{Y}_i = (1/\sqrt{S}) \sum_{\mathbf{q}} (\alpha_{\mathbf{q}, i} \hat{a}_{\mathbf{q}} - \alpha_{\mathbf{q}, i}^* \hat{a}_{\mathbf{q}}^\dagger)$ , while the momentum-space lattice-mode operator transforms as

$$e^{-\mathcal{U}} \hat{a}_{\mathbf{q}} e^{\mathcal{U}} = \hat{a}_{\mathbf{q}} - \frac{1}{\sqrt{S}} \sum_i e^{i\mathbf{q} \cdot \mathbf{R}_i} \alpha_{\mathbf{q}, i}^* \hat{n}_i. \quad (19)$$

By replacing the fields in Eq. (3) with the transformed ones from Eqs. (18) and (19), and choosing  $\alpha_{\mathbf{q}, i} = (g_{AB} \sqrt{n_A}/\epsilon_q) \Lambda_{\mathbf{q}}^{ii}$  to exactly cancel the impurity-lattice-modes interaction, we obtain

$$\begin{aligned} \tilde{K}_B^{\text{eff}} = & -\tilde{J} \sum_{\langle i, j \rangle} \hat{b}_i^\dagger \hat{b}_j + \frac{\tilde{U}}{2} \sum_i \hat{n}_i (\hat{n}_i - 1) - \tilde{\mu}_B \sum_i \hat{n}_i \\ & - \sum_{\langle i, j \rangle} \frac{V_{i, j}}{2} \hat{n}_i \hat{n}_j. \end{aligned} \quad (20)$$

Above, we neglected retardation effects, assuming that the lattice excitations instantaneously follow the motion of a heavy B impurity. Also, to obtain Eq. (20), we traced out the lattice degrees of freedom from the transformed Hamiltonian  $\tilde{K}_B^{\text{eff}} = \langle \tilde{K}_A^{\text{BOG}} + \tilde{K}_B + \tilde{H}_{\text{int}} \rangle_{\text{ph}}$ , with  $|\text{ph}\rangle = \prod_{\mathbf{q}} |N_{\mathbf{q}}\rangle$  and  $|N_{\mathbf{q}}\rangle$  being a number state of the lattice modes [45]. The effective BH parameters for the trapped species B in the presence of the lattice modes read

$$\begin{aligned} \tilde{J} &= J \langle \hat{X}_i^\dagger \hat{X}_j \rangle_{\text{ph}} = \\ &= J \exp \left[ -\frac{g_{AB}^2 n_A}{2S} \sum_{\mathbf{q}} \frac{|\Lambda_{\mathbf{q}}^{ii} (1 - e^{-i\mathbf{q} \cdot (\mathbf{R}_j - \mathbf{R}_i)})|^2}{\epsilon_q^2} \right], \end{aligned} \quad (21)$$

$$\tilde{U} = U - \frac{2n_A g_{AB}^2}{S} \sum_{\mathbf{q}} \frac{|\Lambda_{\mathbf{q}}^{ii}|^2}{\epsilon_q}, \quad (22)$$

$$\tilde{\mu}_B = \mu_B + \frac{n_A g_{AB}^2}{S} \sum_{\mathbf{q}} \frac{|\Lambda_{\mathbf{q}}^{ii}|^2}{\epsilon_q}. \quad (23)$$

Besides changes of the Bose-Hubbard-model parameters ( $J$ ,  $U$ , and  $\mu_B$ ), the lattice dynamics also induces an

attractive long-range potential between the impurities, which is mediated by the lattice modes. This corresponds to the last term in Eq. (20), where

$$V_{i, j} = \frac{2n_A g_{AB}^2}{S} \sum_{\mathbf{q}} \frac{(\Lambda_{\mathbf{q}}^{ii})^* \Lambda_{\mathbf{q}}^{jj}}{\epsilon_q}. \quad (24)$$

Based on the expressions for the Bogoliubov coefficients  $u_{\mathbf{q}}$  and  $v_{\mathbf{q}}$  at small  $q$ , we can estimate the strength  $V_{i, j}$  of the isotropic long-range attraction between atoms on neighboring sites  $i$  and  $j$ , at a lattice distance  $d$ . By using the quadratic Tkachenko-mode dispersion  $\epsilon_q$  [13], we find (see Appendix A for a detailed derivation)

$$V_{i, j} \propto \frac{e^{-d^2/2\ell_0^2}}{d^2}. \quad (25)$$

The strong suppression of  $V_{i, j}$  at large distance justifies considering a truncated model, in which  $V_{i, j} = V$  when  $i$  and  $j$  are nearest neighbors, and  $V_{i, j} = 0$  otherwise. The parameter  $V > 0$  quantifies the strength of the nearest-neighbor attraction, and the departure from the ordinary BH model.

## V. EXTENDED BOSE-HUBBARD PHASE DIAGRAM

In this section, we characterize the phase diagram of the resulting EBH model described in Sec. IV by Eq. (20). We first treat the case of vanishing hopping parameter  $\tilde{J}$  (atomic limit), and we assume  $zV < \tilde{U}$  to guarantee the system stability. For larger values of the nearest-neighbor attraction  $V$ , it is energetically favorable to add an infinite number of particles in the system.

The simplest ground state ansatz is a homogeneous state with  $g$  particles per site:

$$|\Psi_g\rangle = \frac{1}{\sqrt{g!}} \sum_i (\hat{b}_i^\dagger)^g |0\rangle, \quad (26)$$

where  $i$  runs over all lattice sites. By minimizing  $\langle \Psi_g | K_B^{\text{eff}} | \Psi_g \rangle$  with respect to  $g$ , we obtain the ground-state filling factor. The boundary between the regions with  $g$  and  $g+1$  atoms per site is given by

$$\tilde{\mu}_B^{(g, g+1)} = g\tilde{U} - \frac{2g+1}{2} zV, \quad (27)$$

and the resulting phase diagram is represented in Fig. 2. The Mott-insulator regions of the ordinary BH phase diagram ( $V = 0$ ) remain present for all values of  $V$ , but their size and position are modified. The size of each Mott region decreases as  $V$  increases, with the extension of the  $g$ -th region along the  $\mu_B$  axis being equal to  $\tilde{U} - zV$ . Moreover, the phase boundaries have a negative slope as a function of  $V$ . This shift follows from the fact that the nearest-neighbor attraction acts as an additional chemical potential, favoring the addition of more atoms in the lattice.

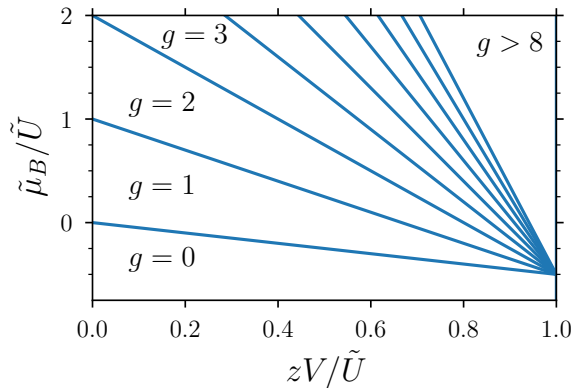


Figure 2. Phase diagram of the EBH model (*cf.* Eq. (20)) in the atomic limit ( $\tilde{J} = 0$ ), formed by Mott-insulator regions with integer filling factor  $g$ . Phase boundaries are obtained through Eq. (27) (regions with filling  $g > 8$  are merged together, for clarity). The system is unstable for  $zV/\tilde{U} > 1$ .

The ansatz  $|\Psi_g\rangle$  cannot reproduce inhomogeneous states, like the charge-density-wave identified for repulsive nearest-neighbor interactions. More general ansätze may be used, that include inhomogeneous state. For instance one can consider the state  $|\Psi_{g_1,g_2,g_3}\rangle$ , with integer filling factors  $g_1, g_2$ , and  $g_3$  on the three sub-lattices represented in Fig. 3. The numerical minimization of the variational energy  $\langle \Psi_{g_1,g_2,g_3} | K_B^{\text{eff}} | \Psi_{g_1,g_2,g_3} \rangle$  leads to  $g_1 = g_2 = g_3$ , implying that the ground state falls in the class of homogeneous states – *cf.* Eqs. (26) and (27). Note that, for repulsive nearest-neighbor interactions (not treated in this work), the tripartite ansatz  $|\Psi_{g_1,g_2,g_3}\rangle$  would also produce ground states with fractional filling factors (e.g., with  $g_1 = 1$  and  $g_2 = g_3 = 0$ ).

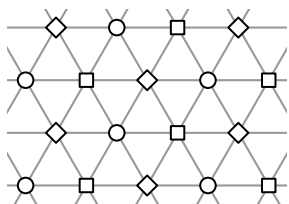


Figure 3. Partition of a triangular lattice into three sub-lattices, represented with different symbols.

For  $\tilde{J} = 0$ , the EBH Hamiltonian is diagonal in the basis of states with fixed filling factors on all sites, so that finding the ground state for a  $L \times L$  finite lattice corresponds to the optimization of a function of  $L^2$  variables (that is, the local occupation numbers). We address this multidimensional optimization problem through the simulated-annealing algorithm [46] for extended systems ( $L \geq 12$ ). The numerical results confirm that the ground state is homogeneous, with filling factor determined by

Eq. (27).

The two variational ansätze and the direct-optimization method employed in the atomic limit cannot be directly generalized to the  $\tilde{J} > 0$  case, where the Hamiltonian also includes off-diagonal terms. To determine the phase diagram in this region (see Fig. 4), we compute the average filling factor (i.e., the density  $\rho$ ) and superfluid fraction  $\rho_s/\rho$  through QMC simulations of large systems at low temperature, effectively probing the ground state. At small  $\tilde{J}/\tilde{U}$ , we observe a direct transition between MI states with different filling factors (*cf.* Fig. 4(a)), with the phase boundaries given approximately by Eq. (27).

For larger values of the hopping coefficient, the transition towards the superfluid phase is signaled by the superfluid fraction acquiring a finite value. The position of this transition, for  $V > 0$ , is well captured by a shifted version of the  $V = 0$  phase boundary. If we denote the critical hopping by  $\tilde{J}/\tilde{U} = f(g, \tilde{\mu}_B/\tilde{U}, V/\tilde{U})$ , then Fig. 4(b) suggests that the simple relation

$$f\left(g, \frac{\tilde{\mu}_B}{\tilde{U}}, \frac{V}{\tilde{U}}\right) = f\left(g, \frac{\tilde{\mu}_B - gzV}{\tilde{U}}, 0\right) \quad (28)$$

holds close to the tips of MI lobes, that is, for large-enough  $\tilde{J}/\tilde{U}$ . The right-hand side in Eq. (28) can be obtained from the process-chain results [39].

## VI. EXPERIMENTAL CONSIDERATIONS

We now discuss the experimental feasibility of our proposal, starting from the criteria on the choice of the mixture. The first required condition is that  $m_B \gg m_A$ , since the lattice potential felt by the impurities (species B) must be deep enough that they can be trapped by the vortex cores. This condition is also fulfilled with  $g_{AB}$  sufficiently large.

For species A, we consider bosonic atoms for which the formation of highly ordered vortex lattices has been observed experimentally [12], namely the alkalis Na, Li, and Rb. We limit our discussion to the commonly explored mixture of  $^{23}\text{Na}$  and  $^{87}\text{Rb}$ , to realize the vortex lattice and heavy impurities, respectively. The BEC lifetime is limited by three-body losses. Requiring that it exceeds a few tens of seconds, we choose  $n_A \approx (10^{20}/\text{m}^3) \times \ell_z$ , with an effective BEC thickness  $\ell_z$  ( $\omega_z \sim 2\pi \times 5$  kHz). Assuming that the bare (non-resonant) scattering length interaction is  $a_A = 60a_0$ , where  $a_0$  is the Bohr radius, the chemical potential reads  $\mu_A = 1.4$  kHz, ( $\sim 70$  nK). To form a vortex lattice that is sufficiently large, homogeneous and stable, we consider similar values for the rotation and the interaction energies  $n_A g_A / 2\hbar\Omega \sim 1$ . At this critical array vorticity  $\Omega$ , the residual radial trap vanishes in Eq. (1) (the harmonic oscillator length of  $V_{\text{ext}}(\mathbf{r})$  coincides with the magnetic length  $\ell = \sqrt{\hbar/(m_A\Omega)}$ ) and one has tightly packed triangular vortex-lattice geometry, with lattice parameter  $d = 2\ell \sim 1.6 \mu\text{m}$  and sites of size  $\xi \sim 0.4 \mu$ .



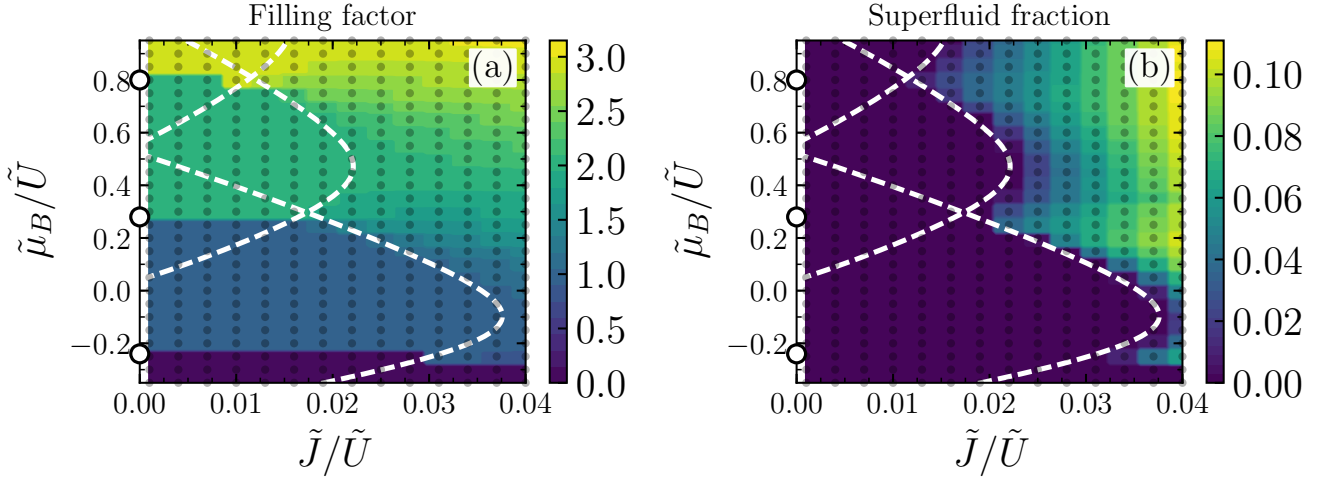


Figure 4. Average filling factor  $\rho$  (a) and superfluid fraction  $\rho_s/\rho$  (b) for the Hamiltonian in Eq. (20), with nearest-neighbor attraction  $V/\tilde{U} = 0.08$ . Color code: QMC data for a lattice of  $18 \times 18$  sites with periodic boundary conditions, at temperature  $T = \tilde{U}/20$  (simulation are performed at points marked by gray dots). Dashed white line: Phase boundaries of the Mott insulators with  $g = 1, 2, 3$ , obtained by shifting the  $V = 0$  data from Ref. [39] – *cf.* Eq. (28).

For species B, the recoil energy  $E_r$  of an impurity localized in the vortex core has to be much smaller than the potential barrier of magnitude  $V_0$ . Taking into account all considerations elaborated above, we find a reasonable value  $V_0/E_r \sim 12$  for  $a_{AB} = 240a_0$ . It is important to stress that with our chosen parameters, the vortex-lattice lifetime can be of the order of several seconds, while the characteristic time associated with the tunnelling  $J$  in Eq. (8) is approximately 0.2 s. In addition, we assume that the occupation in the sites are low enough that the states of the impurities are accurately described using the lowest-band Wannier functions. Reminding that the density of sites  $n_V$  is constraint by  $n_A$  in the high filling-factor regime,  $\nu = N_A/N_V \gg 1$ , the impurities have a negligible influence on the lattice bosons, due to the diluteness of species B ( $n_B \sim n_V$ ).

We can then estimate the characteristic energies for the Bose-Hubbard coefficients of species B in Eq. (5). For the hopping parameter we have  $J \sim 0.004 \mu_A$ . In the two-species vortex-lattice setup, the ratio  $U/J$  can be tuned by changing the scattering length  $a_B$ , as shown by Eq. (9). To access the region of the phase diagram that corresponds to the MI-SF transition, assuming the unitary occupation of the lattice sites, we consider  $a_B^{\text{crit}} \approx 277a_0$ , which gives  $U/J \sim 26.6$ .

The extended Bose-Hubbard (EBH) in Eq. (20), includes an attractive long-range potential with magnitude  $V \sim 0.005 \mu_A$  (*cf.* Eq. (A1) in Appendix A). Importantly, we have  $V/\tilde{U} \sim 0.05$ , which obeys the stability condition for the ground-state solution of the EBH,  $zV/\tilde{U} < 1$ .

Using a  $^7\text{Li}$ - $^{133}\text{Cs}$  mixture would require a magnetic field on the order of 850 G to render the scattering length of  $^7\text{Li}$  positive and sufficiently large. An advantage of this mixture would be the high value of the ratio  $V_0/E_r$  which

could be obtained without significantly increasing  $a_{AB}$ . Working with a more massive impurity than  $^{87}\text{Rb}$  would allow one to realize the MI-SF transition using smaller values for the scattering lengths. The disadvantage, however, would be the higher three-body loss rate estimated for  $^7\text{Li}$  [47], reducing lifetime for the vortex lattice.

## VII. CONCLUSIONS

In the present work, we propose a setup to realize a BH model with a mixture of ultracold atomic gases in the presence of an effective rotation (namely, an artificial gauge-field). Similarly to the typical optical-lattice setups, the tunability of the physical parameters of the system allows to explore a wide range of regimes for the effective BH model. The vortex-lattice Tkachenko modes, in particular, modifies the BH parameters and introduces an additional long-range attraction. The EBH model with long-range repulsion (stemming from strong dipolar interatomic interactions) has been studied in detail, and it led to the prediction of additional phases which are not present in the ordinary BH case, like the density-wave and supersolid phases in two dimensions [48, 49]. For the attractive EBH model in Eq. (20), we compute the phase diagram through the quantum Monte Carlo technique. The Mott-insulator regions of the BH case remain in the extended model, but their size and position are modified by the long-range attraction.

A recent publication [50] treats a similar topic, that is, the phase diagram of impurities in a vortex lattice. However, Ref. [50] concerns the vortex-lattice deformations caused by the strong interaction with the impurity, and how the higher occupation of the sites affects the BH parameters. In this work, in contrast, we studied

the weak-coupling limit, focussing on the interaction of the impurity with the vortex-lattice degrees of freedom. After establishing the stability conditions for a vortex lattice in the presence of multiple impurities, we explored the effects of the lattice dynamics on the confined species. Treating the dilute system by means of an effective polaronic Hamiltonian, we showed how it allows to go beyond the present studies with atoms trapped in static optical lattices.

Besides being part of an unusual BH class, our proposed model is also an interesting experimental proposal in the context of Bose-Einstein condensate mixtures, since it requires the application of the most recent and successful techniques in the ultracold atoms field: The advances in cooling mechanism to produce binary condensates [51], the Feshbach-resonance technique to control the interaction parameters, and artificial gauge-fields to selectively nucleate vortex lattices in one of the atomic species [29]. The possible quantum phases can be characterized through the spatial noise correlations in the absorption image of the free expanded atomic cloud [52]. Similar techniques can be used to observe signatures of more exotic states, such as spin liquids [53].

Fermions could also be considered in this same framework. Using two hyperfine states, interesting effects are

expected to arise in a Mott-insulator phase of the pseudo-spin fermions, with the interplay between the triangular-lattice geometry and spin ordering frustration [16, 54]. In the optical lattice, however, the study of quantum spin models and of strongly-correlated magnetic phases, as the spin-liquid phase, has been limited by the high temperature of the fermions in the lattice, which is still higher than that required to observe exchange-driven spin ordering. In our case, in contrast, the BEC vortex-lattice background can act like a reservoir, with the cooling of the trapped fermions coming from the creation of excitations in this reservoir. This favorable scenario was proposed in the context of dissipative Hubbard models [55], where the strong control over many parameters, as interactions between atoms, allows one to manipulate the system-reservoir coupling.

## ACKNOWLEDGMENTS

We thank Marco Di Liberto for insightful comments, and Martin Holthaus for providing the data from Ref. [39]. This work is supported by CNPq and FAPESP.

- 
- [1] W. Zwerger, in *The BCS-BEC Crossover and the Unitary Fermi Gas (Lecture Notes in Physics)* **836**, Springer (2011).
  - [2] I. Bloch, J. Dalibard, and S. Nascimbène, *Nat. Phys.* **8**, 267 (2012).
  - [3] O. Mandel, M. Greiner, A. Widera, T. Rom, T. W. Hänsch, and I. Bloch, *Nature* **425**, 937 (2003).
  - [4] C. J. Myatt, E. A. Burt, R. W. Ghrist, E. A. Cornell, and C. E. Wieman, *Phys. Rev. Lett.* **78**, 586 (1997).
  - [5] M. R. Matthews, B. P. Anderson, P. C. Haljan, D. S. Hall, C. E. Wieman, and E. A. Cornell, *Phys. Rev. Lett.* **83**, 2498 (1999).
  - [6] V. Schweikhard, I. Coddington, P. Engels, S. Tung, and E. A. Cornell, *Phys. Rev. Lett.* **93**, 210403 (2004).
  - [7] R. P. Feynman, *Prog. Low Temp. Phys.* **1**, 17 (1955).
  - [8] V. K. Tkachenko, *J. Exp. Theor. Phys.* **56**, 1763 (1969).
  - [9] J. R. Abo-Shaeer, C. Raman, J. M. Vogels, and W. Ketterle, *Science* **292**, 476 (2001).
  - [10] I. Coddington, P. Engels, V. Schweikhard, and E. A. Cornell, *Phys. Rev. Lett.* **91**, 100402 (2003).
  - [11] V. Schweikhard, I. Coddington, P. Engels, V. P. Mogenдорff, and E. A. Cornell, *Phys. Rev. Lett.* **92**, 040404 (2004).
  - [12] A. Fetter, *Rev. Mod. Phys.* **81**, 647 (2009).
  - [13] M. A. Caracanhas, V. S. Bagnato, and R. G. Pereira, *Phys. Rev. Lett.* **111**, 115304 (2013).
  - [14] M. Greiner, M. O. Mandel, T. Esslinger, T. Hänsch, and I. Bloch, *Nature* **415**, 39 (2002).
  - [15] D. Jaksch, C. Bruder, J. I. Cirac, C. W. Gardiner, and P. Zoller, *Phys. Rev. Lett.* **81**, 3108 (1998).
  - [16] M. Lewenstein, A. Sanpera, and V. Ahufinger, *Ultracold Atoms in Optical Lattices: Simulating quantum many-body systems*, Oxford University Press (2012).
  - [17] A. Griessner, A. J. Daley, S. R. Clark, D. Jaksch, and P. Zoller, *New J. Phys.* **9**, 44 (2007).
  - [18] A. Klein, M. Bruderer, S. R. Clark, and D. Jaksch, *New J. Phys.* **9**, 411 (2007).
  - [19] M. Bruderer, A. Klein, S. R. Clark, and D. Jaksch, *Phys. Rev. A* **76**, 011605(R) (2007).
  - [20] K. Góral, L. Santos, and M. Lewenstein, *Phys. Rev. Lett.* **88**, 170406 (2002).
  - [21] E. G. Dalla Torre, E. Berg, and E. Altman, *Phys. Rev. Lett.* **97**, 260401 (2006).
  - [22] T. Lahaye, C. Menotti, L. Santos, M. Lewenstein, and T. Pfau, *Rep. Prog. Phys.* **72**, 126401 (2009).
  - [23] C. Trefzger, C. Menotti, B. Capogrosso-Sansone, and M. Lewenstein, *J. Phys. B: At. Mol. Opt. Phys.* **44**, 193001 (2011).
  - [24] S. Baier, M. J. Mark, D. Petter, K. Aikawa, L. Chomaz, Z. Cai, M. Baranov, P. Zoller, and F. Ferlaino, *Science* **352**, 201 (2016).
  - [25] C. Chin, R. Grimm, P. Julienne, and E. Tiesinga, *Rev. Mod. Phys.* **82**, 1225 (2010).
  - [26] R. Landig, L. Hruby, N. Dogra, M. Landini, R. Mottl, T. Donner, and T. Esslinger, *Nature* **532**, 476 (2016).
  - [27] J. T. Stewart, J. P. Gaebler, and D. S. Jin, *Nature* **454**, 744 (2008).
  - [28] J. Dalibard, F. Gerbier, G. Juzeliūnas, and P. Öhberg, *Rev. Mod. Phys.* **83**, 1523 (2011).
  - [29] I. B. Spielman, *Phys. Rev. A* **79**, 063613 (2009).
  - [30] S. I. Matveenko, D. Kovrizhin, S. Ouvry, and G. V. Shlyapnikov, *Phys. Rev. A* **80**, 063621 (2009).
  - [31] S. I. Matveenko, and G. V. Shlyapnikov, *Phys. Rev. A* **83**, 033604 (2011).



- [32] J. Sinova, C. B. Hanna, and A. H. MacDonald, Phys. Rev. Lett. **89**, 030403 (2002).
- [33] I. Bloch, J. Dalibard, and W. Zwerger, Rev. Mod. Phys. **80**, 885 (2008).
- [34] A. Fetter, in *Lectures in Theoretical Physics* vol. **XIB**, p. 351, Gordon and Breach, New York (1969).
- [35] W. Zwerger, J. Opt. B: Quantum Semiclassical Opt. **5**, S9 (2003).
- [36] M. P. A. Fisher, P. B. Weichman, G. Grinstein, and D. S. Fisher, Phys. Rev. B **40**, 546 (1989).
- [37] K. V. Krutitsky, Phys. Rep. **607**, 1 (2016).
- [38] D. van Oosten, P. van der Straten, and H. T. C. Stoof, Phys. Rev. A **63**, 053601 (2001).
- [39] N. Teichmann, D. Hinrichs, and M. Holthaus, EPL **91**, 10004 (2010).
- [40] N. Teichmann, D. Hinrichs, M. Holthaus, and A. Eckardt, Phys. Rev. B **79**, 224515 (2009).
- [41] A. F. Albuquerque *et al.* (ALPS collaboration), J. of Magn. and Magn. Materials **310**, 1187 (2007).
- [42] B. Bauer *et al.*, J. Stat. Mech.: Theory Exp., P05001 (2011).
- [43] D. Benjamin, and E. Demler, Phys. Rev. A **89**, 033615 (2014).
- [44] K. Agarwal, I. Martin, M. Lukin, and E. Demler, Phys. Rev. B **87**, 144201 (2013).
- [45] See section 4.31 and 4.32 of G. D. Mahan, *Many-Particle Physics* Plenum, New York, 3rd (2000).
- [46] S. Kirkpatrick, C. D. Gelatt Jr. and M. P. Vecchi, Science, **220**, 671 (1983).
- [47] N. Gross, Z. Shotan, S. Kokkelmans, and L. Khaykovich, Phys. Rev. Lett. **103**, 163202 (2009).
- [48] C. Trefzger, C. Menotti, and M. Lewenstein, Phys. Rev. A **78**, 043604 (2008).
- [49] J.-Y. Gan, Y.-C. Wen, and Y. Yu, Phys. Rev. B **75**, 094501 (2007).
- [50] T. H. Johnson, Y. Yuan, W. Bao, S. R. Clark, C. Foot, and D. Jaksch, Phys. Rev. Lett. **116**, 240402 (2016).
- [51] C. C. Tannoudji, and D. G. Odelin, in *Advances in Atomic Physics: An Overview*, World Scientific (2011).
- [52] E. Altman, E. Demler, and M. D. Lukin, Phys. Rev. A **70**, 013603 (2004).
- [53] R. Bach, and K. Rzażewski, Phys. Rev. Lett. **92**, 200401 (2004).
- [54] D. Greif, T. Uehlinger, G. Jotzu, L. Tarruell, and T. Esslinger, Science **340**, 1307 (2013).
- [55] A. Griessner, A. J. Daley, S. R. Clark, D. Jaksch, and P. Zoller, New J. Phys. **79** 44 (2007).
- [56] N. V. Prokof'ev, B. V. Svistunov, and I. S. Tupitsyn, Phys. Lett. A **238**, 253 (1998).
- [57] J. Šmakov, and E. & Sørensen, Phys. Rev. Lett. **95**, 180603 (2005).

## Appendix A: Mediated potential

Based on the Bogoliubov transformation of the vortex-lattice [31], we can determine the profile of the long-range effective potential given by Eq. (24) in the main text. In particular, its asymptotic behavior can be estimated analytically with the low-energy (long-wavelength) Tkachenko modes contribution, as will be shown.

As studied before [13], for  $q \ll \ell^{-1}$ , with the magnetic length  $\ell$  related to the inter-vortex separation through  $d = 2\ell$ , the gapless Tkachenko modes have dispersion relation  $\epsilon_q \approx \hbar^2 q^2 / 2M$ , with  $M = \frac{1}{2\kappa\sqrt{\eta}} \frac{\hbar\Omega}{n_A g_A} m_A$  and the lattice constant  $\kappa = 1.1592$  and  $\eta = 0.8219$ . In the low-energy limit, we have  $u_{\mathbf{q}}(\mathbf{r}) \approx \varphi_A(\mathbf{r}) c_{1\mathbf{q}} e^{i\mathbf{q}\cdot\mathbf{r}}$  and  $v_{\mathbf{q}}(\mathbf{r}) \approx \varphi_A(\mathbf{r}) c_{2\mathbf{q}} e^{-i\mathbf{q}\cdot\mathbf{r}}$ . The small value of the momentum allows us to expand  $(c_{1q} - c_{2q}) \approx \frac{1}{\sqrt{2}} \eta^{1/4} (q\ell)$ .

According to the Extended Bose-Hubbard Hamiltonian (Eq. (20)), we can determine the profile of the mediated potential from Eq. (15), assuming again the gaussian function for  $\varphi_B(r) (= |B_0| e^{-r^2/2\ell_0^2})$

$$\begin{aligned}
 V_{i,j} = V(d) &\sim \frac{2n_A g_{AB}^2}{S} \sum_{\mathbf{q}} \frac{\left[ \frac{1}{\sqrt{2}} \eta^{1/4} (q\ell) \right]^2}{\epsilon_q} \left[ \int d^2r |B_0|^2 e^{-|\mathbf{r}-\mathbf{d}|^2/2\ell_0^2} e^{-r^2/2\ell_0^2} \right]^2 \\
 &= \frac{g_{AB}^2}{g_A} \frac{1}{\kappa} |B_0|^4 e^{-d^2/\ell_0^2} \int_0^{2\pi/\ell} q dq \left[ \int r dr e^{-r^2/\ell_0^2} \int_0^{2\pi} d\theta e^{r d \cos \theta / \ell_0^2} \right]^2 \\
 &= \frac{g_{AB}^2}{g_A} \frac{4\pi}{\kappa} \frac{1}{d^2} e^{-d^2/2\ell_0^2}.
 \end{aligned} \tag{A1}$$

This result justifies the restriction of the potential range to nearest-neighboring sites.

## Appendix B: Details of the quantum Monte Carlo calculations

The quantum Monte Carlo simulations in this work make use of the worm algorithm [56], as implemented in the ALPS libraries [41, 42]. For the bosonic models in Eqs. (5) and (20), this represents an unbiased method to compute observables as the density or energy, at finite temperature  $T$  and for a finite number of sites  $L^2$ .

The phase boundary showed in Fig. 1 is obtained through the finite-size scaling technique [36], by finding the critical hopping parameter  $J_{\text{crit}}$  for fixed  $U$  and  $\mu_B$ . Away from the tip of the Mott-insulator lobe, a *generic* phase transition

is expected, with dynamical and correlation-length critical exponents equal to 2 and 1/2, respectively [36, 37]. Under this assumption, and for  $J$  close to  $J_{\text{crit}}$ , the superfluid stiffness  $\rho_s$  satisfies

$$L^2 \rho_s = F \left( \frac{J_{\text{crit}} - J}{J_{\text{crit}}} L^2, \frac{1}{L^2 T} \right), \quad (\text{B1})$$

where  $F$  is a universal function. Thus  $J_{\text{crit}}$  can be obtained by plotting  $L^2 \rho_s$  as a function of  $J$  for several linear sizes  $L$ , at fixed  $T \times L^2$ , and by extracting the common intersection point of these lines (see for instance Ref. [57]). When rescaled as in Eq. (B1), superfluid-stiffness lines corresponding to different values of  $L$  collapse onto a single curve, confirming the correct estimate of the critical value  $J_{\text{crit}}$  – see the example in Fig. 5.

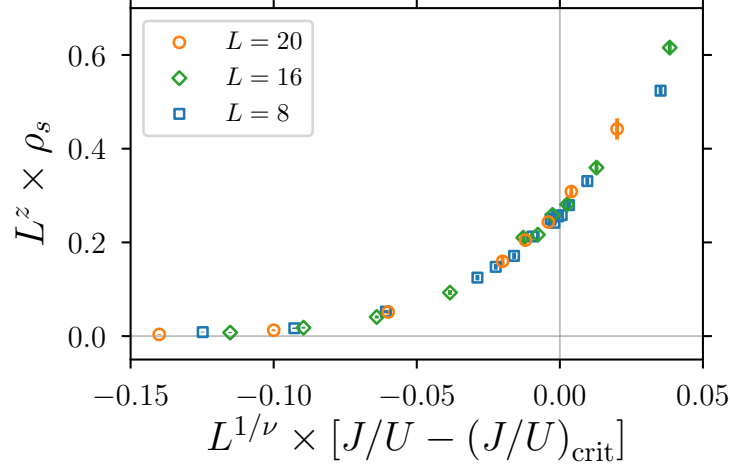


Figure 5. Data collapse of the superfluid stiffness  $\rho_s$ : Data for different linear sizes  $L$  (see legend) are rescaled as in Eq. (B1), with  $z = 2$  and  $\nu = 1/2$  being the dynamical and correlation-length critical exponents. With the product  $T \times L^z$  kept equal to 0.5, different lines collapse onto a single universal curve. Data are shown for chemical potential  $\mu_B/U = 0.645$ , with  $(J/U)_{\text{crit}} = 0.02595$ .